First-principles calculations of intrinsic defects in Al_2O_3

Katsuyuki Matsunaga
Institute of Engineering Innovation, The University of Tokyo, 2-11-16, Yayoi, Bunkyo-ku, Tokyo 113-8656, Japan

Tomohito Tanaka and Takahisa Yamamoto
Department of Advanced Materials Science, Graduate School of Frontier Sciences, The University of Tokyo, 2-11-16, Yayoi, Bunkyo-ku, Tokyo 113-8656, Japan

Yuichi Ikuhara
Institute of Engineering Innovation, The University of Tokyo, 2-11-16, Yayoi, Bunkyo-ku, Tokyo 113-8656, Japan
(Received 25 March 2003; published 25 August 2003)

First-principles plane-wave pseudopotential calculations were performed to study electronic structures, structural relaxation, and energetics of intrinsic vacancies and interstitials in Al_2O_3. In the presence of the intrinsic point defects, extra levels appeared in the band gap. Considering various charge states for the intrinsic point defects, it was found that each point defect is most stable in its fully ionized state. From the formation energies of individual point defects, Schottky, O Frenkel, and Al Frenkel energies were also evaluated and were compared with previous results by experiment and static lattice calculations. Although previous static lattice calculations showed different relative stabilities of Schottky and Frenkel formation, depending on the choice of interatomic potentials, our calculations revealed that the relative values of formation energies are in the order of Schottky$<$Al Frenkel$<$O Frenkel, which is in good agreement with experimental data.

DOI: 10.1103/PhysRevB.68.085110 PACS number(s): 61.72.Bb, 61.72.Ji, 71.15.Mb

I. INTRODUCTION

Al_2O_3 with the corundum structure has a wide variety of technological applications such as high-temperature structural ceramics, dielectric insulators, and optical devices. This is due to the fact that this material has excellent mechanical properties, good chemical inertness, and electronic structures suitable for microelectronics and laser optics. Many of these properties are closely related to point defects and impurities introduced in bulk Al_2O_3. For instance, diffusion of vacancies or interstitials plays a crucial role for the high-temperature mechanical properties of Al_2O_3.[1–6] Optical transmission of Al_2O_3 also depends on a small concentration of impurities and color centers.[7] It is, therefore, very important to understand structures and chemistry of point defects in Al_2O_3.

Based on the requirement of charge neutrality and stoichiometry, possible intrinsic defects in Al_2O_3 can be simply classified into Schottky-type or Frenkel-type defects. For intrinsic defects in Al_2O_3, Mohapatra and Kröger reported from thermodynamic data that the formation energy of Schottky defects (two Al^{3+} and three O^{2-} vacancies) was 3.83 eV per defect, while that of cation Frenkel defects (one interstitial Al^{3+} and one Al^{3+} vacancy) was 4.45 eV per defect, indicating that Schottky defects are dominant in bulk Al_2O_3.[8] In contrast, intrinsic defects in Al_2O_3 were also theoretically studied mainly by using empirical and semi-empirical methods.[9–12] Dienes *et al.*[9] performed shell-model calculations based on ionic potentials for intrinsic vacancies and interstitials in Al_2O_3. The authors showed that the formation of Schottky defects is energetically more favorable than that of cation- or anion-Frenkel defects, which is consistent with the above experimental results. However, more recent atomistic simulations[10–12] showed that oxygen Frenkel defects have a lower formation energy than Schottky defects. There is a discrepancy between these results by atomistic simulations as to which is a dominant defect type in Al_2O_3. As pointed out by Catlow *et al.*,[10] this may be due to the difference in potential parameters used for describing properties of Al_2O_3. Potential parameters for atomistic simulations are generally determined from perfect crystal properties such as cohesive energy, equilibrium lattice constants, and bulk modulus. Thus it is not easy to conclude whether the potential parameters being used are appropriate for defect calculations or not. It can be expected, however, that ions around defects are present in different chemical environments from those in the perfect lattice, which should be correctly taken into account for evaluating the defect-formation energies.

Recently, first-principles calculations, which are more accurate computational techniques, have been performed for isolated defects in metal oxide.[13–16] Energetics, lattice relaxation, and characteristic electronic structures of defects can be explored by using a large supercell, without a particular choice of interatomic interactions around defects. However, a limited number of theoretical studies on intrinsic defects in Al_2O_3 have been reported. This may be because the corundum structure is rather complex, and its defect calculations require significant computational time and resources. Xu *et al.* employed the orthogonalized linear combination of atomic orbitals (OLCAO) method to study the electronic structures and formations energies of neutral and charged oxygen vacancies in Al_2O_3.[17] They found that these vacancies introduced defect levels occupied by electrons in the band gap, and the optical transitions between the defect level and excited states were in good agreement with available experimental data. Tanaka *et al.* also carried out first-principles calculations of a neutral oxygen vacancy in Al_2O_3

using a plane-wave-basis pseudopotential method.[18] They also calculated neutral oxygen vacancies in several oxides and pointed out a correlation between defect-formation energies and defect-induced levels located around band gaps. Although these studies provide physical insight into the oxygen vacancy in Al_2O_3, other possible intrinsic defects such as Al vacancy and interstitials have not been considered. It cannot be, therefore, theoretically concluded which type of defect formation is energetically favorable in pure Al_2O_3.

In this study, a first-principles pseudopotential method was used to study electronic structures, atomic geometries, and formation energies of intrinsic defects in Al_2O_3. The formation energies of isolated intrinsic defects were calculated by using large supercells. Possible defect reactions such as Schottky and Frenkel types were considered, and their formation energies were compared with available experimental and simulated results.

II. COMPUTATIONAL METHODS

A. Pseudopotentials and supercells for α-Al_2O_3

First-principles calculations of intrinsic defects in Al_2O_3 were performed using a plane-wave pseudopotential method as implemented in the VASP code.[19–22] For the exchange-correlation potential, the generalized gradient approximation (GGA) was employed, and the GGA functional given by Perdew and Wang was used.[23] Forces on atoms were calculated, and atoms were allowed to relax using a conjugate gradient technique until their residual forces had converged to less than 0.1 eV/Å.

In order to reduce the number of plane-wave basis functions necessary for accurately describing electronic wave functions, ultrasoft Vandelbilt pseudopotentials implemented in VASP were used.[24] The ultrasoft pseudopotential for Al was generated from the atomic configuration of $[\mathrm{Ne}]3s^2 3p^1$, and the $3s^2$ and $3p^1$ electrons were treated as valence electrons. The core radius was taken to be 2.65 a.u. (1 a.u. $=0.529$ Å). For O, the reference configuration for the ultrasoft pseudopotential was $[\mathrm{He}]2s^2 2p^4$ with a core radius of 1.55 a.u., and the $2s^2$ and $2p^4$ electrons were considered as valence electrons. Although these core radii for Al and O result in a slight core overlap in the bulk and defect structures of Al_2O_3, a number of previous studies demonstrated the transferability of Vanderbilt pseudopotentials even using large core radii.[24–26] To check the applicability and accuracy of the above pseudopotentials, calculations of perfect Al_2O_3 were carried out. For the rhombohedral primitive unit cell of α-Al_2O_3, which has $R\bar{3}c$ symmetry and contains two Al_2O_3 formula units, Brillouin-zone integrations were made by a $4\times4\times4$ k-point mesh (ten irreducible k points) generated according to the Monkhorst-Pack scheme.[27] In this case, a plane-wave cutoff energy (E_{cut}) of 500 eV was used. It was confirmed that the total energy at 500 eV was converged less than 0.1 meV/atom with respect to that at 700 eV. Optimized values of a_{rho} (lattice parameter), α_{rho} (an angle between lattice vectors), and u_{Al} and v_{O} (internal parameters for Al and O) are listed in Table I. Our calculated values are in good agreement with experiment.[28] It is noted that the lattice parameter a_{rho} obtained in this study is slightly larger than those obtained by experiment and previous calculations[29–32] with the local density approximation (LDA). This is due to the use of the GGA in the present study. Separate LDA calculations of α-Al_2O_3 were also performed with the exchange-correlation function of Ceperley and Alder as parameterized by Perdew and Zunger.[33] By using the similar conditions for pseudopotentials, k-space integration, and E_{cut}, it was found that the present LDA results agree with the ones by other researchers, as shown in Table I. Such trends in theoretical lattice parameters by the GGA were also pointed out for other oxide systems.[34,35]

TABLE I. Calculated structural parameters for α-Al_2O_3 and their comparison with previous theoretical and experimental results.

		a_{rho} (Å)	α_{rho} (deg)	u_{Al}	v_{O}
This work	GGA	5.195	55.32	0.353	0.306
	LDA	5.111	55.37	0.352	0.306
Ref. 29		5.086	55.30	0.352	0.306
Ref. 30		5.107	55.41	0.352	0.305
Ref. 31		5.123	55.43	0.352	0.306
Ref. 32		5.045	57.23	0.355	0.312
Experimental[a]		5.136	55.28	0.352	0.306

[a]Reference 28.

Based on the optimized structural parameters for the perfect crystal, Al_2O_3 supercells were constructed for defect calculations. Figure 1 displays an Al_2O_3 supercell used in this study. The supercell containing 120 atoms is in the hexagonal lattice with dimensions of $a_0=9.65$ Å and $c_0=13.16$ Å. To introduce an isolated vacancy, an interior Al or O atom is removed from the supercell. In the case of an isolated interstitial, an atom of Al or O is put into the supercell, where the normally vacant octahedral site in the Al sublattice is considered as a possible interstitial site. For calculations of the defective supercells, atoms located within a radius of 3.4 Å from defects were allowed to relax. In this radius for relaxation, atoms within third-nearest-neighbor (3NN) sites are present for vacancies, while those within 4NN sites for interstitials. In order to check an effect of

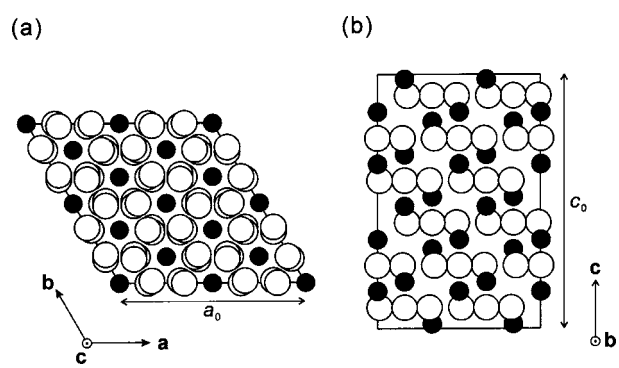

FIG. 1. Structure of Al_2O_3 supercell containing 120 atoms used in the present study. Solid circles indicate Al atoms, while open circles O atoms. (a) and (b) are the top view along the ***c*** axis and the side view along ***b*** axis, respectively.

relaxation cutoff radius on defect formation energies, supercell calculations with a larger relaxation cutoff (3.6 Å) were also performed for oxygen interstitial. This is because an oxygen interstitial has a large ionic size and thus may induce large relaxation of surrounding atoms. It was found that the formation-energy difference between relaxation cutoff radii of 3.4 and 3.6 Å was less than 0.1 eV, which does not affect the present results significantly. Numerical integrations over Brillouin zone were performed only at the Γ point because of the large size of supercells. An E_{cut} value was selected to be 500 eV for all supercell calculations. It was confirmed that total energies of defective supercells at $E_{\mathrm{cut}}=500$ eV were converged within 1.5 meV/atom relative to those at $E_{\mathrm{cut}}=700$ eV.

B. Defect formation energies

The formation energies of intrinsic defects in Al_2O_3 were calculated from the total energies of defective supercells based on the standard formalism by Zhang and Northrup.[36] In the case of Al_2O_3, the formation energies of intrinsic defects depend on the chemical potentials of Al and O, and also vary with electronic chemical potential (namely, the Fermi level) if a defect has a charge of q. For a defect with a charge q (including its sign), its formation energy (H_f) is given by

$$H_f=E_T(\mathrm{defect};q)-N_{\mathrm{Al}}\mu_{\mathrm{Al}}-N_{\mathrm{O}}\mu_{\mathrm{O}}+q(\varepsilon_F+E_{\mathrm{VBM}}). \tag{1}$$

where $E_T(\mathrm{defect};q)$ is a total energy of a supercell with the defect, and N_{Al} and N_{O} are the numbers of Al and O atoms in the defective supercell. μ_{Al} and μ_{O} are chemical potentials of Al and O atoms, respectively. ε_F is the Fermi energy measured from the valence-band maximum (VBM). In a supercell calculation for an isolated point defect, Eq. (1) can be rewritten in terms of a total energy of the perfect Al_2O_3 supercell [$E_T(\mathrm{perfect})$] as follows:

$$H_f=E_T(\mathrm{defect};q)-\{E_T(\mathrm{perfect})+n_{\mathrm{Al}}\mu_{\mathrm{Al}}+n_{\mathrm{O}}\mu_{\mathrm{O}}\}+q(\varepsilon_F+E_{\mathrm{VBM}}). \tag{2}$$

Here n_{Al} and n_{O} are the numbers of Al and O atoms removed from or added to the perfect supercell to introduce a vacancy or interstitial. For example, $n_{\mathrm{Al}}=-1$ and $n_{\mathrm{O}}=0$ for an Al vacancy, and $n_{\mathrm{Al}}=+1$ and $n_{\mathrm{O}}=0$ for an Al interstitial. For each defect species, its charge q varying from neutral to fully ionized states was considered: $-3\sim\pm0$ for an Al vacancy (V_{Al}), $\pm0\sim+2$ for an O vacancy (V_{O}), $\pm0\sim+3$ for an Al interstitial (Al_i), and $-2\sim\pm0$ for an O interstitial (O_i).

As can be seen in Eq. (2), E_{VBM} should be determined from supercell calculations in order to obtain the formation energy of a charged defect. However, the position of E_{VBM} in the defective supercell is in general different from that in the perfect supercell. This is due to the finite size of supercells and the effects of background charge for neutralizing supercells with charged defects.[37–40] Therefore, it is necessary to line up band structures of the perfect and defective supercells. For this purpose, E_{VBM} values of defective supercells were obtained from the one of the perfect supercell and a difference in average potentials (V_{av}) between the perfect supercell and a bulklike environment (far from the defect) in defective supercells as follows:[39,40]

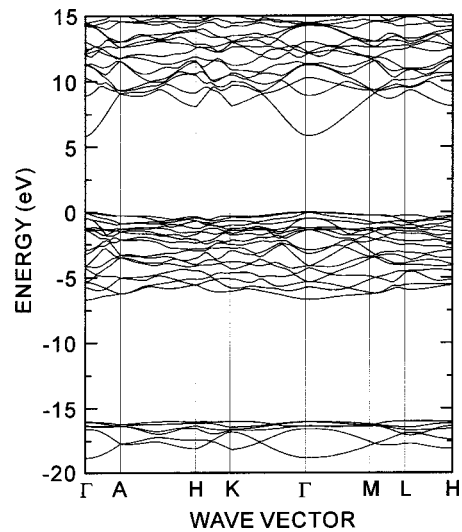

FIG. 2. Band structure for α-Al_2O_3 along symmetry lines of the hexagonal irreducible Brillouin zone. The valence-band maximum is set at 0 eV.

$$E_{\mathrm{VBM}}=E_{\mathrm{VBM}}^{\mathrm{perfect}}+V_{\mathrm{av}}^{\mathrm{defect}}-V_{\mathrm{av}}^{\mathrm{perfect}}. \tag{3}$$

The first term of the right-hand side of Eq. (3) can be obtained by

$$E_{\mathrm{VBM}}^{\mathrm{perfect}}=E_T(\mathrm{perfect};0)-E_T(\mathrm{perfect};+1), \tag{4}$$

where $E_T(\mathrm{perfect};0)$ is the total energy of the neutral perfect supercell [namely, $=E_T(\mathrm{perfect})$ in Eq. (2)]. $E_T(\mathrm{perfect};+1)$ is that of the $+1$ charged perfect supercell, which corresponds to the situation that one electron is removed from the VBM of the neutral perfect supercell.

The Fermi level of ε_F in Eq. (1) varies from the VBM to the conduction-band minimum (CBM), therefore, in a range of the band gap value (E_g). However, GGA (and also LDA) calculations usually underestimate E_g as compared to experimental data. From the calculated band structure of perfect Al_2O_3 (Fig. 2), it is found that the E_g value at the Γ point is 5.82 eV, which is much smaller than the experimental one of 8.7 eV.[41,42] This difference between theory and experiment ($\Delta E_g=2.88$ eV) could affect formation energies of intrinsic defects in Al_2O_3.[43] When a defect induces extra occupied levels below the CBM, which are composed of cation orbitals similar to the conduction band, its formation energy will be underestimated since the energy position of the CBM itself is underestimated. This situation corresponds to oxygen vacancy and Al interstitial in Al_2O_3, which will be shown later. In such cases, it was assumed as crude correction that the conduction band is rigidly shifted upward to match the experimental E_g. Then formation energies were corrected by adding a value of $m\times\Delta E_g$, where m is the number of electrons at defect-induced levels in E_g.[43]

μ_{Al} and μ_{O} in Eq. (2) are not independent, but are constrained by the equilibrium condition of $2\mu_{\mathrm{Al}}+3\mu_{\mathrm{O}}$

$=\mu_{Al2O3}$, where μ_{Al2O3} is a total energy per molecule of perfect Al_2O_3. Although μ_{Al} and μ_O can vary under the equilibrium condition, upper limits of μ_{Al} and μ_O are determined by the stability limit of Al_2O_3 in terms of total energies for metallic Al and molecular O_2 in the following manner:

$$\mu_{Al} \leqslant \mu_{Al}^0, \quad \mu_O \leqslant \mu_O^0, \tag{5}$$

where μ_{Al}^0 and μ_O^0 are total energies per atom of metallic Al and molecular O_2, respectively. Also, the formation enthalpy ($\Delta H_f^{Al_2O_3}$) can be obtained by

$$\Delta H_f^{Al2O3} = 2(\mu_{Al} - \mu_{Al}^0) + 3(\mu_O - \mu_O^0). \tag{6}$$

From Eqs. (5) and (6), the range of μ_O is represented as

$$\frac{1}{3}\Delta H_f^{Al_2O_3} + \mu_O^0 \leqslant \mu_O \leqslant \mu_O^0. \tag{7}$$

Here $\mu_O = \mu_O^0$ and $\mu_O = 1/3\Delta H_f^{Al_2O_3} + \mu_O^0$ correspond to the oxidation and reduction limits, respectively.

In order to obtain the range of μ_O, separate calculations of the total energies of metallic Al with fcc structure and molecular O_2 were performed. For metallic Al, a $14\times14\times14$ Monkhorst-Pack mesh (280 irreducible k points) and $E_{cut} = 500$ eV were used. The optimized lattice parameter was 4.04 Å, which agrees well with an experimental one of 4.05 Å.[44] For O_2, an isolated O_2 molecule was placed in a cubic cell with the dimension of $15\times15\times15$ Å^3. In this case, only the Γ point was used. The O-O bond length of 1.24 Å thus obtained was in good agreement with experiment (1.21 Å).[45] The resulting formation enthalpy of Al_2O_3 obtained from Eq. (6) was -16.71 eV/Al_2O_3, which is comparable to the experimental value of -17.37 eV/Al_2O_3.[45]

III. RESULTS AND DISCUSSION

A. Electronic structures of isolated defects

As a typical example, calculated densities of states (DOS) at the Γ point for the defect-free supercell and those containing four kinds of neutral isolated defects are shown in Fig. 3. In this figure, the VBM for each DOS, which was determined from corrections by average potentials as described in Sec. II B, was set at 0 eV. The highest occupied levels in the DOS of defective supercells are depicted by the arrows.

In the VB structure of perfect Al_2O_3 [Fig. 3(a)], the lower O 2s band is located at around $-20\sim-16$ eV, while the upper O 2p band at about $-7\sim0$ eV. Beyond E_g (=5.82 eV), the CB composed of Al 3s and 3p bands is present. These VB features are consistent with previous theoretical results.[17,18,32]

As can be seen from Figs. 3(b)–3(e), the overall DOS profiles for defective supercells are quite similar to that of perfect Al_2O_3. However, extra levels can be observed at around VB or CB edges of the band gap E_g. In the case of V_{Al}^0 [Fig. 3(b)], its highest occupied level with one electron is located at 0.3 eV, and one unoccupied level is also present at the same energy. It can be said, therefore, that V_{Al}^0 introduces

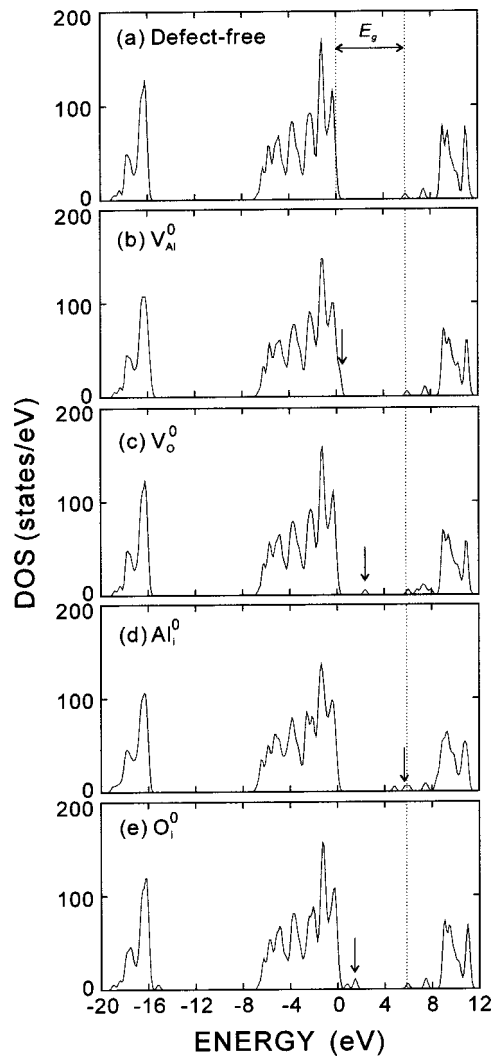

FIG. 3. Densities of states at the Γ point for defect-free and defective supercells. The valence-band maxima are set at 0 eV. The highest occupied levels for the defective supercells are denoted by arrows.

acceptorlike levels at the vicinity of the VBM. In contrast, V_O^0 [see Fig. 3(c)] induces the highest level occupied by two electrons at 2.3 eV, as indicated by the arrow. As will be shown later, this level is composed of Al 3s orbitals, and thus comes from the CBM in the presence of V_O^0. Such a deep level in E_g due to V_O^0 was also found in previous first-principles studies.[17,18]

In the case of Al_i^0, two extra levels appear in the upper part of E_g [see Fig. 3(d)]; the level at 4.78 eV is occupied by two electrons, while the one at 5.71 eV by one electron. For O_i^0 [Fig. 3(e)], extra levels are introduced close to the VBM. Its highest occupied level with two electrons is situated at 1.43 eV, and another unoccupied one is also located at the same energy. The presence of the highest occupied level around the VB edge is similar to the case of V_{Al}^0. However, its energy position is higher than that of V_{Al}^0.

In order to investigate features of the highest occupied levels in the defective supercells, contour plots of squares of

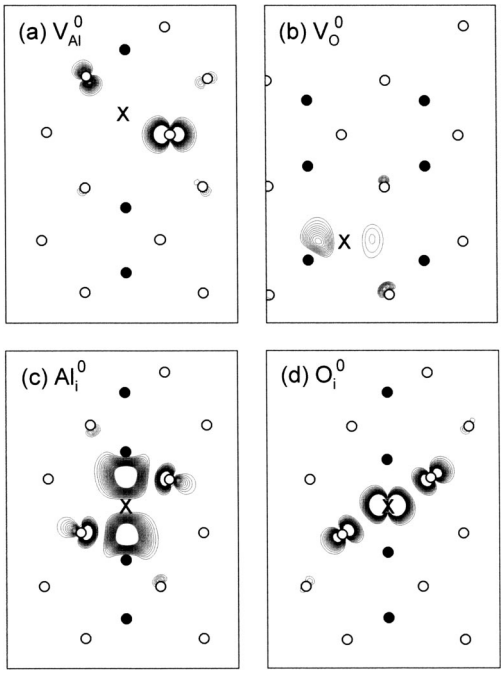

FIG. 4. Contour maps of wave functions of defect levels on an $\{11\bar{2}0\}$ plane of the corundum structure. The contour lines are from 0.04 to 0.2 with an interval of 0.01 in units of electrons/Å^3. Solid and open circles indicate positions of Al and O ions, respectively. The position of each defect species is represented by "X."

their wave functions on an $\{11\bar{2}0\}$ plane are shown in Fig. 4. As can be seen, these levels have distributions almost within second nearest neighbors from the defect positions. This indicates that these levels are induced by the presence of the defects and thus are called as "defect levels" hereafter.

From Fig. 4(a), the defect level by V_{Al}^0 is composed of O $2p$ orbitals neighboring the vacancy. Since the defect level has similar orbital components with the upper VB of perfect Al_2O_3, it can be understood that this level is located very close to the VBM as shown in Fig. 3(b). In contrast, the defect level by V_O^0 [Fig. 4(b)] is constructed mainly by neighboring Al $3s$ orbitals. It is noteworthy that the Al $3s$ orbitals adjacent to V_O^0 extend to the vacancy, indicating significant localization at the vacancy site. Although Al $3s$ orbitals make the conduction band in perfect Al_2O_3, such localization of Al $3s$ orbitals at the defect level brings about a considerable energy shift downward from the CB edge, resulting in the formation of the deep defect level in E_g as is seen in Fig. 3(c).

For Al_i^0 and O_i^0, contour maps of their defect levels are more complicated than those of V_{Al}^0 and V_O^0. The defect level by Al_i^0 [Fig. 4(c)] is constructed mainly by combination of Al_i $3s$ and neighboring Al $3s$ orbitals. Due to such Al $3s$ orbital character, this defect level is situated at the CB edge as shown in Fig. 3(d). It is noted here that O $2p$ orbitals in this level also interact with Al $3s$ orbitals in an antibonding manner, so that this level does not become a deep defect level in E_g, unlike that of V_O^0. In the case of O_i^0, its defect level is constructed by O_i $2p$ and adjacent O $2p$ orbitals with antibonding interactions. Although this level has similar orbital character with the upper VB, therefore, such antibonding interactions give rise to its energy shift upward from the VB edge, which can be clearly seen in Fig. 3(e).

As stated above, intrinsic defects in Al_2O_3 induce defect levels around the VB and CB edges in the band gap. Since structural relaxation also takes place around a defect, the distances between a defect and surrounding atoms after structural relaxation were examined. Results for defects with various charge states are summarized in Table II. It is noted that atoms in a certain coordination shell do not always have the same distance from a defect site, which is due to the low symmetry of the corundum structure. For example, an Al vacancy site has six O ions at 1.88 and 2.00 Å as 1NN ions before relaxation. In such a case, the average value of 1.94 Å is shown in this table.

In the presence of V_{Al}^0, it can be seen that 1NN O ions exhibit outward relaxation of about 7%, while 2NN Al ions show inward relaxation of about 4%. This can be understood in terms of ionic size and charge effects. When an Al atom is removed to form the vacancy, 1NN O ions are no longer electrostatically attracted to the vacancy and therefore move away from the vacancy. In contrast, 2NN Al ions move closer to the vacancy since electrostatic repulsions of Al-Al are reduced by the vacancy formation. When negative charge states of V_{Al} increase, 2NN Al ions undergo more inward relaxations due to the electrostatic attraction between V_{Al} and 2NN Al ions. As compared to the 2NN Al ions, however, the distances between V_{Al} and 1NN O ions do not change so much with rising charge states of V_{Al}. Since O ions with a large ionic size are subject to significant electrostatic repulsions with surrounding O ions, it is thought that O ions are energetically more difficult to relax than Al ions, even in the presence of the charged defects.

For V_O^0, 1NN Al ions move toward the vacancy by about 1.5%, and 2NN O ions show slight inward relaxation of about 0.4%. Such inward relaxation of 1NN Al ions is contrary to the case of V_{Al}^0. This can be attributed to the large ionic size of oxygen. When an O atom is removed, attractive interactions of 1NN Al ions with the O atom are missing, but alternatively an open space is formed at the V_O site. Due to the open space by the V_O formation, 1NN Al ions with a small ionic size can slightly relax toward the vacancy. It is noted, however, that 1NN Al ions for V_O with higher charge states move farther away from the vacancy. In the case of V_O^{2+}, it is found that 1NN Al ions show an outward relaxation of 9.7%. This can be explained by the electrostatic repulsions between 1NN Al ions and V_O with a positive effective charge.

In perfect Al_2O_3, the interstitial site has two 1NN Al ions at 1.94 Å and six 2NN O ions at 2.00 Å. When Al_i^0 is introduced, Al and O ions surrounding it undergo significant outward relaxation of more than 7%. As can be seen from Table II, six O ions are located at 2.15 Å as 1NN ions of Al_i^0 and two Al ions at 2.20 Å as 2NN ions. With increasing positive charge states of Al_i, six O ions come closer to Al_i, and their distances become similar to Al-O bond lengths in perfect

TABLE II. Structural relaxation around each defect species. Average distances from the defect positions to neighboring atoms are listed. Neighboring atomic species and their coordination numbers are also shown in parentheses.

	Distance in Å (atomic species, coordination number)			
	1 NN	2 NN	3 NN	4 NN
Al (bulk Al_2O_3)	1.94(O;6)	2.80(Al;4)	3.26(Al;3), 3.26(O;3)	
V_{Al}^{0}	2.08(O;6)	2.69(Al;4)	3.25(Al;3), 3.26(O;3)	
V_{Al}^{1-}	2.08(O;6)	2.67(Al;4)	3.23(Al;3), 3.27(O;3)	
V_{Al}^{2-}	2.07(O;6)	2.63(Al;4)	3.20(Al;3), 3.29(O;3)	
V_{Al}^{3-}	2.08(O;6)	2.59(Al;4)	3.16(Al;3), 3.29(O;3)	
O (bulk Al_2O_3)	1.94(Al;4)	2.76(O;12)	3.26(Al;2)	
V_{O}^{0}	1.91(Al;4)	2.75(O;12)	3.26(Al;2)	
V_{O}^{1+}	2.03(Al;4)	2.72(O;12)	3.26(Al;2)	
V_{O}^{2+}	2.13(Al;4)	2.68(O;12)	3.27(Al;2)	
Interstitial (bulk Al_2O_3)	1.94(Al;2)	2.00(O;6)	2.80(Al;6)	3.34(O;6)
Al_i^{0}	2.15(O;6)	2.20(Al;2)	2.88(Al;6)	3.36(O;6)
Al_i^{1+}	1.90(O;6)	2.26(Al;2)	2.89(Al;6)	3.31(O;6)
Al_i^{2+}	1.89(O;6)	2.27(Al;2)	2.89(Al;6)	3.31(O;6)
Al_i^{3+}	1.88(O;6)	2.28(Al;2)	2.89(Al;6)	3.30(O;6)
O_i^{0}	1.89(Al;2)	2.17(O;6)	2.84(Al;6)	3.33(O;6)
O_i^{1-}	1.80(Al;2)	2.22(O;6)	2.81(Al;6)	3.34(O;6)
O_i^{2-}	1.70(Al;2)	2.28(O;6)	2.78(Al;6)	3.34(O;6)

Al_2O_3 (1.88 and 2.00 Å), while two Al ions move farther away from Al_i due to the electrostatic repulsions of Al and Al_i.

Unlike the case of Al_i, it is found that the distance from O_i^0 to 1NN Al becomes smaller by 2.6%, as compared to that in perfect Al_2O_3. This is reasonable since the distance of O_i^0-1NN Al (1.89 Å) is close to the Al-O bond lengths in perfect Al_2O_3. However, the 2NN O ions undergo outward relaxations of more than 10%, especially with rising negative charge states of O_i.

B. Formation energies

Figure 5 shows formation energies H_f for isolated defects in Al_2O_3 as a function of the Fermi level ε_F. As stated in Sec. II B, H_f values also vary with atomic chemical potentials. In this figure, calculated results in the oxidation limit ($\mu_O = \mu_O^0$) are plotted. It can be seen that the most stable charge states of respective defect species depend on the position of ε_F. For instance, when ε_F is near E_{VBM} (close to 0 eV), the stable charge state for each defect can be represented as V_{Al}^0, V_O^{2+}, Al_i^{3+}, and O_i^0. On the other hand, when ε_F is located close to E_{CBM}, V_{Al}^{3-}, V_O^0, Al_i^{1+}, and O_i^{2-} are the most stable. These two situations of ε_F correspond to *p*-type and *n*-type electronic environments induced by dopants, respectively, as often found in extrinsic semiconductors. In this case, an insulating system of pure Al_2O_3 is considered, and thus the Fermi level can be selected at the midpoint of E_g.[15]

It can be seen from Fig. 5 that the highest charge states for respective defect species are most stable at $\varepsilon_F = E_g/2$: namely, V_{Al}^{3-}, V_O^{2+}, Al_i^{3+}, and O_i^{2-}. This can be understood from the ionic picture of Al_2O_3, where Al_2O_3 is constructed by Al^{3+} and O^{2-} ions and thus vacancies and interstitials formed are also fully ionized. Among these stable defects, V_{Al}^{3-} exhibits a negative H_f value, indicating that this

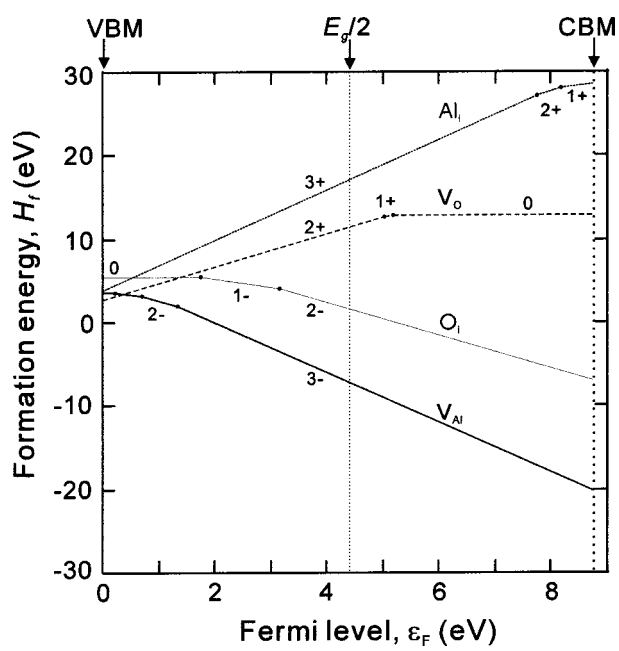

FIG. 5. Formation energies of intrinsic point defects as a function of the Fermi level ε_F at the oxidation limit. For each defect species, only the lowest-energy charge states with respect to ε_F are shown. The zero energy of ε_F corresponds to the valence-band minimum, while the vertical dotted line at 8.7 eV indicates the conduction-band minimum using the experimental E_g value.

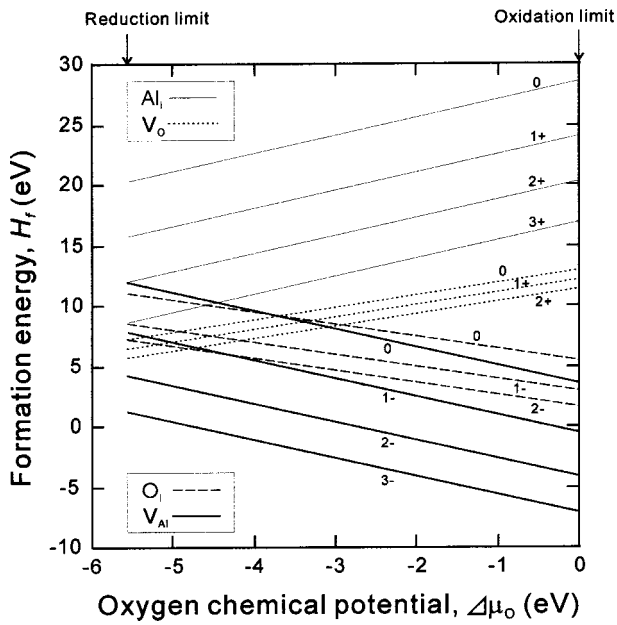

FIG. 6. Calculated formation energies for individual point defects against the oxygen chemical potential ($\Delta\mu_O = \mu_O - \mu_O^0$) at $\varepsilon_F = E_g/2$.

defect is easy to form. O_i^{2-} also has a small positive H_f value (1.68 eV) as compared to Al_i^{3+} and V_O^{2+}. The relatively high value of H_f for Al_i^{3+} can also be imagined from the large lattice distortions as shown in Table II.

Figure 6 displays variations of H_f as a function of μ_O. As μ_O shifts from the oxidation limit to the reduction limit, based on Eq. (2) and the equilibrium condition of $2\mu_{Al} + 3\mu_O = \mu_{Al_2O_3}$, H_f values of Al_i and V_O are found to decrease, while those of V_{Al} and O_i increase. For all defect species, their highest charge states still exhibit the smallest formation energies. It is also found that the relative stability of the charged defects is $V_{Al}^{3-} < O_i^{2-} < V_O^{2+} < Al_i^{3+}$ in a wide range of μ_O. When μ_O is close to the reduction limit, however, the H_f of V_O^{2+} becomes smaller than that of O_i^{2-}.

As shown above, intrinsic defects in Al_2O_3 are stable in their fully ionized charge states. Although electronic defects to compensate defect charges may be formed at very high temperatures, these can be considered to be minor defect species. In addition, Al_2O_3 is a stoichiometric material, and thus the formation of Schottky and Frenkel pairs comprising the charged point defects according to charge neutrality has to be taken into account. In this case, the Schottky quintet of $2V_{Al}^{3-} + 3V_O^{2+}$, the O Frenkel pair of $O_i^{2-} + V_O^{2+}$ and the Al Frenkel pair of $Al_i^{3+} + V_{Al}^{3-}$ can be considered. The H_f values for individual charged point defects in Figs. 5 and 6 were then combined to give the Schottky and Frenkel formation energies as shown in Table III. It is noted here that the Schottky and Frenkel energies are independent of μ_O, since the whole system of Al_2O_3 is still stoichiometric even after their formation.

From Table III, the Schottky quintet has a smaller formation energy per defect, as compared to those of O Frenkel and Al Frenkel pairs. In addition, the formation energy of Al Frenkel pairs is smaller than that of O Frenkel pairs. Mohapatra and Kröger experimentally suggested that the Schottky quintet is dominant in Al_2O_3.[8] Their reported enthalpies of Schottky and Al Frenkel formation per defect were 3.83 and 4.45 eV, respectively, which are close to our calculated values.

In contrast, previous theoretical results using static lattice calculations showed different relative stability between the Schottky and Frenkel defects from one another. Dienes *et al.*[9] reported that the Schottky defects are most stable, and yet O Frenkel defects have a smaller formation energy than Al Frenkel pairs. Catlow *et al.* employed two types of pair potentials for Al_2O_3; one was derived from empirical fitting to bulk crystal properties and the other from the electron-gas model.[10] The former provided the relative stability of O Frenkel < Schottky < Al Frenkel. Similar results were also found in the recent static lattice calculations by Grimes[11] and Lagerlöf and Grimes.[12] However, the latter showed the relative stability was in the order of Schottky < Al Frenkel < O Frenkel, whose trend is consistent with our results although their absolute values are much higher (see Table III). Therefore, defect-formation energies obtained by static lattice calculations are very sensitive to interatomic potentials used, which is not conclusive to determine a dominant defect structure in Al_2O_3. This may be because many of the inter-

TABLE III. Calculated Schottky and Frenkel formation energies in Al_2O_3. The values obtained by static lattice calculations and experiment are also shown, for comparison.

	Formation energy per defect (eV)		
	Schottky quintet	O Frenkel pair	Al Frenkel pair
This work	4.01	6.52	4.95
Static lattice calc.			
Ref. 9	5.7	7.0	10.0
Ref. 10 (empirical)	4.70	4.06	6.47
(electron-gas model)	5.14	8.27	7.09
Ref. 11	5.86	5.79	6.30
Ref. 12	5.17	4.87	6.59
Experiment[a]	3.83	-	4.45

[a]Reference 8.

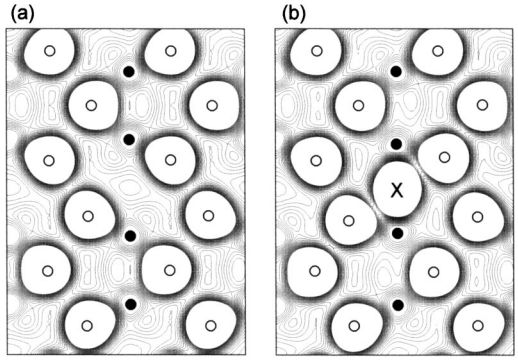

FIG. 7. Contour maps of total valence electron densities on an $\{11\bar{2}0\}$ plane of the corundum structure: (a) the perfect Al_2O_3 and (b) the $O_{1'}^{2-}$ supercells. The contour lines are from 0.02 to 0.4 with an interval of 0.02 in units of electrons/Å^3. Solid and open circles indicate positions of Al and O ions, respectively. The position of O_i^{2-} is represented by "X" in (b).

atomic potentials were obtained by reference to perfect crystal properties. For instance, an interstitial ion has different atomic coordination from an ion at a normal lattice site, and its interactions with neighboring ions are more complex than those between ions at normal sites. Figure 7 shows contour maps of the total valence electron densities for perfect Al_2O_3 and O_i^{2-} obtained in this study. The electron densities between Al and O at normal sites exhibit a typical ionic character of bonding. It can be seen, however, that electron densities of O_i^{2-} undergo significant distortion due to interactions with their neighboring ions. Such electronic interactions will affect its defect-formation energy. Although a complementary theoretical technique such as the Mott-Littleton method[46] was included for atomistic simulations to take into account electronic polarization around defects, it is likely that detailed electronic interactions around defects have to be treated in a first-principles manner, so as to obtain quantitative defect-formation energies.

The present calculations indicate that the relative values of the formation energies are of the order of Schottky $<$Al Frenkel$<$O Frenkel. It should be noted, however, that the calculated values in Table III are for the situation that individual point defects explicitly have no interactions with each other. In order to conclude whether the Schottky defect is most stable in Al_2O_3 or not, it is necessary to consider a possibility of defect association. This is because individual point defects in Al_2O_3 have nonzero effective charges as shown in Fig. 5, which will give rise to their electrostatic interactions. In addition, each point defect induces lattice distortions around it, and thus elastic interactions between point defects will be present. Hence further supercell calculations were performed for defect complexes of O_i^{2-}-V_O^{2+} and Al_i^{3+}-V_{Al}^{3-}, which correspond to O Frenkel and Al Frenkel associated pairs, respectively. In this case, it was assumed that a vacancy is present at the 1NN site of an interstitial, and the defect complexes were placed at around the center of supercells as shown in Fig. 1. Structural relaxation was also performed for ions within 3.4 Å from each point defect.

TABLE IV. Calculated formation energies of associated Frenkel pairs in Al_2O_3.

Defect complex	Formation energy per defect (eV)
O_i-V_O	5.69
Al_i-V_{Al}	4.50

Table IV lists calculated formation energies of the O_i^{2-}-V_O^{2+} and Al_i^{3+}-V_{Al}^{3-} complexes. The formation energy of O_i^{2-}-V_O^{2+} is smaller by 0.83 eV than that in Table III, indicating significant stabilization of the Frenkel pair by association. Likewise, the Al_i^{3+}-V_{Al}^{3-} complex exhibits a smaller formation energy due to association, whose value of 4.50 eV is in good agreement with experimental data (4.45 eV). It should be noted here that the Schottky formation energy obtained in Table III is still smallest even by taking into account the defect association of these two Frenkel defects. Although the defect association of the Schottky quintet was not treated in the present study, it is conceivable that the association will also contribute to decrease its formation energy, resulting in its more comparable formation energy with experiment than that shown in Table III.

The present calculations showed that the Schottky defects are dominant in pure Al_2O_3. In contrast, Lagerlöf *et al.*[3] and Heuer and Lagerlöf[4] suggested that Al or O interstitials may play an important role for the diffusion mechanism of undoped Al_2O_3. Since point-defect concentrations in undoped Al_2O_3 are expected to be relatively small due to their high formation energies, it is plausible that their concentrations in real undoped Al_2O_3 may depend on the presence of a small amount of impurities such as Mg, Ca, and Si. Such effects of impurities on the point-defect chemistry in Al_2O_3 are important to understand its mass-transport and optical properties, which will be done using a similar first-principles method.

IV. SUMMARY

First-principles pseudopotential calculations were performed to study electronic structures and formation energies of intrinsic defects in Al_2O_3. The results obtained in this study can be summarized as follows.

(1) In the presence of vacancies and interstitials for Al and O, extra levels were induced around valence-band or conduction-band edges in the band gap of Al_2O_3. In the case of the neutral oxygen vacancy (V_O^0), a deep defect level was formed at around the midpoint of the band gap. This is due to that this wave function composed of Al 3*s* orbitals is strongly localized at the vacancy site.

(2) Various charge states for individual point defects were considered, and their formation energies were calculated. For all defect species, the fully ionized states of V_{Al}^{3-}, V_O^{2+}, Al_i^{3+}, and O_i^{2-} were found to be most stable in pure Al_2O_3.

(3) Based on the above results, formation energies of the Schottky and Frenkel defects, which maintain charge neutral-

ity and stoichiometry of Al_2O_3, were evaluated. It was found that the calculated formation energies exhibit good agreement with available experimental data, and the Schottky defects have the smallest formation energy.

(4) By taking into account defect association, further calculations of Al and O Frenkel pairs were performed. Their formation energies decreased by defect association and yet were larger than that of the Schottky defect. This indicates that the Schottky defects are dominant in pure Al_2O_3, which is consistent with experiment.

ACKNOWLEDGMENTS

This work was supported by a Grant-in-Aid for Scientific Research and Special Coordination Funds from the Ministry of Education, Culture, Sports, Science and Technology of the Japanese government.

[1] R. M. Cannon, W. H. Rhodes, and A. H. Heuer, J. Am. Ceram. Soc. **63**, 46 (1980).
[2] A. H. Heuer, N. J. Tighe, and R. M. Cannon, J. Am. Ceram. Soc. **63**, 53 (1980).
[3] K. P. D. Lagerlöf, T. E. Mitchell, and A. H. Heuer, J. Am. Ceram. Soc. **72**, 2159 (1989).
[4] A. H. Heuer and K. P. D. Lagerlöf, Philos. Mag. Lett. **79**, 619 (1999).
[5] X. Tang, K. P. D. Lagerlöf, and A. H. Heuer, J. Am. Ceram. Soc. (to be published).
[6] H. Yoshida, Y. Ikuhara, and T. Sakuma, Acta Mater. **50**, 2955 (2002).
[7] B. D. Evans, J. Appl. Phys. **70**, 3995 (1991).
[8] S. K. Mohapatra and F. A. Kröger, J. Am. Ceram. Soc. **61**, 106 (1978).
[9] G. J. Dienes, B. O. Welch, C. R. Fisher, R. D. Hatcher, O. Lazareth, and M. Samberg, Phys. Rev. B **11**, 3060 (1975).
[10] C. R. A. Catlow, R. James, W. C. Mackrodt, and R. F. Stewart, Phys. Rev. B **25**, 1006 (1982).
[11] R. W. Grimes, J. Am. Ceram. Soc. **77**, 378 (1994).
[12] K. P. D. Lagerlöf and R. W. Grimes, Acta Mater. **46**, 5689 (1998).
[13] A. F. Kohan, G. Ceder, D. Morgan, and C. G. Van der Walle, Phys. Rev. B **61**, 15 019 (2000).
[14] S. B. Zhang, S. H. Wei, and A. Zunger, Phys. Rev. B **63**, 075205 (2001).
[15] C. Kılıç and A. Zunger, Phys. Rev. Lett. **88**, 095501 (2002).
[16] R. Astala and P. D. Bristowe, Modell. Simul. Mater. Sci. Eng. **9**, 415 (2001).
[17] Y. N. Xu, Z. Q. Gu, X. F. Zhong, and W. Y. Ching, Phys. Rev. B **56**, 7277 (1997).
[18] I. Tanaka, K. Tatsumi, M. Nakano, H. Adachi, and F. Oba, J. Am. Ceram. Soc. **85**, 68 (2002).
[19] G. Kresse and J. Hafner, Phys. Rev. B **47**, R558 (1993).
[20] G. Kresse, Ph.D. thesis, Technische Universität Wien, 1993.
[21] G. Kresse and J. Furthmüller, Comput. Mater. Sci. **6**, 15 (1996).
[22] G. Kresse and J. Furthmüller, Phys. Rev. B **54**, 11 169 (1996).
[23] J. P. Perdew, J. A. Chevary, S. H. Vosko, K. A. Jackson, M. R. Pederson, D. J. Singh, and C. Fiolhais, Phys. Rev. B **46**, 6671 (1992).
[24] D. Vanderbilt, Phys. Rev. B **41**, 7892 (1990).
[25] K. Laasonen, R. Car, C. Lee, and D. Vanderbilt, Phys. Rev. B **43**, 6796 (1991).
[26] A. Christensen and E. A. Carter, J. Chem. Phys. **114**, 5816 (2001).
[27] H. J. Monkhorst and J. D. Pack, Phys. Rev. B **13**, 5188 (1976).
[28] H. d'Amour, D. Schiferl, W. Denner, H. Schulz, and W. B. Holzapfer, J. Appl. Phys. **49**, 4411 (1978).
[29] A. G. Marinopoulos and C. Elsässer, Acta Mater. **48**, 4375 (2000).
[30] W. Duan, R. M. Wentzcovitch, and K. T. Thomson, Phys. Rev. B **57**, 10 363 (1998).
[31] J. C. Boettger, Phys. Rev. B **55**, 750 (1997).
[32] W. Y. Ching and X. N. Xu, J. Am. Chem. Soc. **77**, 404 (1994).
[33] J. P. Perdew and A. Zunger, Phys. Rev. B **23**, 5048 (1981).
[34] J. Goniakowski, J. M. Holender, L. N. Kantorovich, and M. J. Gillan, Phys. Rev. B **53**, 957 (1996).
[35] G. Jomard, T. Petit, A. Pasturel, L. Magaud, G. Kresse, and J. Hafner, Phys. Rev. B **59**, 4044 (1999).
[36] S. B. Zhang and J. E. Northrup, Phys. Rev. Lett. **67**, 2339 (1991).
[37] D. B. Laks, C. G. Van de Walle, G. F. Neumark, P. E. Blöchl, and S. T. Pantelides, Phys. Rev. B **45**, 10 965 (1992).
[38] A. García and J. E. Northrup, Phys. Rev. Lett. **74**, 1131 (1995).
[39] S. Pöykkö, M. J. Puska, and R. M. Nieminen, Phys. Rev. B **53**, 3813 (1996).
[40] T. Mattila and A. Zunger, Phys. Rev. B **58**, 1367 (1998).
[41] R. H. French, J. Am. Chem. Soc. **73**, 477 (1990).
[42] M. L. Boltz and R. H. French, Appl. Phys. Lett. **55**, 1955 (1989).
[43] S. B. Zhang, S. H. Wei, A. Zunger, and H. Katayama-Yoshida, Phys. Rev. B **57**, 9642 (1998).
[44] C. Kittel, *Introduction to Solid State Physics*, 6th ed. (Wiley, New York, 1986).
[45] D. R. Lide, *CRC Handbook of Chemistry and Physics* (CRC Press, New York, 1998).
[46] N. F. Mott and M. J. Littleton, Trans. Faraday Soc. **34**, 485 (1938).